Title: A peptide that regulates metalation and function of the *Arabidopsis* ethylene receptor

Authors:
Anna J. Mudge[1]†, Saher Mehdi[1]††, Will Michaels[1,2]†, Beatriz Orosa-Puente[1]‡, Weiran Shen[1], Ari Sadanandom[1], Flora M. Hetherington[1]‡‡, Claudia Hoppen[3], Buket Uzun[3], Georg Groth[3], Jennifer F. Topping[1], Nigel J. Robinson[1,2*], Keith Lindsey[1*]

Affiliations:
[1]*Department of Biosciences, Durham University, Durham, UK*
[2]*Department of Chemistry, Durham University, Durham, UK*
[3]*Institute of Biochemical Plant Physiology, Heinrich Heine University Düsseldorf, D-40204 Düsseldorf, Germany*

†These authors contributed equally to this work
††Present address: wellOwise Research and Development, IIITD Innovation & Incubation Centre, New Delhi, Delhi - 110020, India.
‡Present address: School of Biological Sciences, University of Edinburgh, Edinburgh EH9 3FF, UK.
‡‡Present address: University of Bath, Claverton Down, Bath BA2 7AY, U.K.
*Joint corresponding authors: keith.lindsey@durham.ac.uk; nigel.robinson@durham.ac.uk

Abstract:
Ethylene signalling represents one of the classic hormonal pathways in plants, with diverse roles in development and stress responses. The dimeric ethylene receptor localizes to the endoplasmic reticulum (ER) and contains Cu(I) ions essential for ethylene binding and signalling. As for other vesicular cupro-proteins, the final step of Cu(I) maturation at the ER is undefined. We previously discovered that mutants in the *Arabidopsis* gene *POLARIS* (*PLS*), encoding a 36 amino acid peptide, exhibit constitutive ethylene signalling responses. Here we report a 1:2 thiol-dependent Cu(I):PLS_2 complex, with an affinity of 3.79 (±1.5) x10^{19} M^{-2}. We demonstrate PLS interactions with the transmembrane domain of receptor protein ETR1, the Cu(I) chaperones ATX1 and CCH, and Cu(I)-transporting P_{1B}-type ATPase RAN1 at the ER. Formation of Cu(I)-dependent PLS-cuproprotein adducts at the ER provides a mechanism to modulate the metalation of ETR1, thereby regulating its activity and representing a novel mechanism for plant hormone receptor regulation.

One Sentence Summary: The POLARIS peptide of *Arabidopsis* regulates activity of the ethylene hormone receptor by controlling Cu(I) availability.

Main text

Ethylene is used by plants as a gaseous hormone to regulate many aspects of development and responses to biotic and abiotic stresses (*1*). It is perceived by a family of receptors that, in *Arabidopsis*, comprises 5 members, ETR1 (ETHYLENE RESPONSE 1), ERS1 (ETHYLENE RESPONSE SENSOR 1), ERS2, ETR2, and EIN4 (ETHYLENE-INSENSITIVE 4) (*2-5*) located on the endoplasmic reticulum (ER) (*6, 7*). The receptors are related to bacterial two-component systems (*2*), form dimers through disulphide bonding at the N-terminal hydrophobic domains (*8, 9*) and contain Cu(I) ions bound to residues Cys65 and His69, essential for ethylene binding and

signal transduction (*10, 11*). In the absence of ethylene these receptors activate a negative regulator CTR1 (CONSTITUTIVE TRIPLE RESPONSE 1), a mitogen-activated protein kinase kinase kinase (MAPKKK), so preventing ethylene responses (*12, 13*). Mechanisms by which receptor activity is regulated are not well understood. We describe here a molecular mechanism of the PLS peptide, and a proposed model for its role in plant development.

Introduction of copper to the ER and ethylene receptor requires the RAN1 (RESPONSIVE TO ANTAGONIST1) protein. This is a predicted copper-transporting P-type ATPase homologous to the yeast Ccc2p and to human Menkes and Wilson disease proteins (*14*). Strong loss-of-function mutants of *RAN1* in *Arabidopsis* (e.g. *ran1-3*, *ran1-4*) exhibit a constitutive ethylene signalling response (*15*), consistent with a loss of receptor function, and similar to higher order loss-of-function receptor mutants, which also show an ethylene hypersignalling phenotype (*16*). Mechanisms of copper homeostasis, post-RAN1 but pre-ETR1, are unknown, and indeed this is true for other compartmentalized cuproproteins supplied with copper, for example via Ccc2p, Menkes or Wilson ATPases.

Results

The POLARIS peptide is a negative regulator of ethylene responses

The *POLARIS* gene of *Arabidopsis* (AT4G39403) encodes a 36 amino acids peptide (Fig. 1a) that, in light-grown seedlings, is most strongly expressed in the root tip and vascular tissues (*17*). We have previously shown that the loss-of-function *pls* mutant is phenotypically similar to *ran1* loss-of-function alleles and *ctr1*, exhibiting a triple response phenotype (short hypocotyl and root, exaggerated apical hook, radial expansion) in the dark in the absence of ethylene (*18*), and a short root in light-grown seedlings (Fig. 1b). Transgenic complementation of the mutant and overexpression of the *PLS* gene suppresses the mutant phenotype, but fails to suppress the *ctr1* mutant phenotype, indicating that the PLS peptide acts upstream of CTR1 (*18*). The *pls* mutant phenotype is rescued by the gain-of-function ethylene resistant mutation *etr1-1* and pharmacological inhibition of ethylene signalling by silver ions (*18*). Ethylene gas production in the *pls* mutant is at wildtype levels, indicating the peptide plays a role in ethylene signalling rather than biosynthesis (*18*). RNA-seq on loss-of-function *pls* mutant and gain-of-function *PLS* transgenic overexpressor (PLSOx) seedlings shows that the *pls* mutant expresses no full length PLS coding sequence, while the PLSOx seedlings express ca. 18-fold higher levels of *PLS* transcript compared to wild-type (Fig. S1; Table S1). Gene Ontology (GO) analysis following RNA-seq transcriptomics of *pls* mutant seedlings shows the up-regulation of genes associated with responses to hormone signalling, biotic and abiotic defence responses, and cell death (Table S1; Fig. S2a). Eighty-four of 353 known ethylene-related genes are significantly up-regulated in the *pls* mutant compared to wildtype, and genes down-regulated in *pls* include categories associated with root morphogenesis, root epidermal cell differentiation, hormone biosynthetic processes, response to nutrients and metal ion transport (Fig. S2; *19*). In PLSOx overexpressors, up-regulated genes include those associated with hormone responses, biotic and abiotic stress responses and cell death; while 169 of 1615 genes associated with response to hormone stimulus are down-regulated compared to wildtype (Fig. S2c, d; *19*). Genes associated with metal ion transport are also down-regulated in PLSOx seedlings (Fig. S2d; *19*). Twenty-four ethylene-related genes are both up-regulated in the *pls* mutant and down-regulated in the PLS-overexpressor, compared with wild-type (Fig. 1c; *19*). This is consistent with a role for PLS in ethylene responses and other, potentially related, signalling, stress and developmental processes.

To further understand the relationship between PLS peptide structure and function, and to investigate conservation of PLS function between species, we carried out synthetic peptide

feeding experiments using hydroponically grown seedlings. The *Arabidopsis* relative *Camelina sativa* contains a gene with partial sequence identity to the *Arabidopsis PLS* gene, encoding a predicted peptide sequence that is 22 amino acids long and identical to the N-terminal 22 amino acids of the *Arabidopsis* PLS except for a phenylalanine to serine substitution at position nine (Fig. 1a). We synthesized full-length PLS peptide, PLS(FL) and truncated versions from both *Arabidopsis* and *C. sativa* (Fig. 1a), and supplied the peptides to *Arabidopsis pls* mutant seedlings hydroponically. The full-length peptides from both *Arabidopsis* and *C. sativa* were each able to rescue the short primary root length of the *Arabidopsis pls* mutant (Fig. 1D), similar to transgenic overexpression and genetic complementation (*17, 18*). PLS(FL) peptide effects on root growth appear to be dose-dependent, as indicated both by genetic studies (*17*) and peptide feeding (Fig. S3a). However, neither a 9 amino acids sequence (N2, Fig. 1e) from the N-terminus, nor C-terminal sequences of 14 (C1) or 24 (C2) amino acids from *Arabidopsis* PLS were able to rescue the mutant (Fig. 1e). Imaging showed that a fluorescent tagged (5-carboxyfluorescein, 5-FAM) version of the *Arabidopsis* N-terminal 22 amino acids sequence of the peptide (N1) is taken up by the roots, and also rescues the mutant root phenotype (Fig. S3b, c).

PLS localizes to the endoplasmic reticulum

Since genetic studies suggest that PLS acts close to the ethylene receptor (*18*), we hypothesized that it should localize to the same subcellular compartment. The ethylene receptor in *Arabidopsis* is localized to the ER (*12*), and ER localization of a proPLS::PLS:GFP fusion protein was confirmed by co-localization with the ER marker dye ER-Tracker™ (Fig. 2a-c) and with an ER-targeted red fluorescent protein RFP-HDEL (*20*) in transgenic plants (Fig. 2g-i). proPLS::PLS:GFP also appears to localize to the nucleus (Fig. 2). As controls, free GFP protein expressed under the control of the PLS promoter is not co-localized to the ER (Fig. 2d-f) and, as expected, the Golgi marker SH:GFP does not co-localize with ER Tracker (Fig. 2m-o). *Trans*-Golgi-localized SULFOTRANSFERASE1 (ST1) mCherry (*21*) show proPLS::PLS:GFP does not localize to the Golgi (Fig. 2j-l). To further clarify the side of the ER membrane on which PLS localizes, transient expression of redox-sensitive GFP (roGFP2) fusions of PLS were carried out. The different excitation properties of roGFP2 in an oxidizing (ER lumen) or reducing environment (cytosol) allows discrimination of the precise location of PLS. Ratiometric analysis and comparison with proteins of known localization revealed that PLS resides at the cytosolic side of the ER and is not localized in the ER lumen (Fig. 2p).

PLS interacts with the ethylene receptor protein ETR1

We hypothesized that PLS plays a role in receptor function and investigated whether this involved direct interaction with the receptor complex. Preliminary experiments using yeast 2-hybrid analysis suggested that PLS interacts with ETR1 (Fig. S4). Confirmation of the physical interaction between PLS and ETR1 in plants came from co-immunoprecipitation (Co-IP) analysis. *Agrobacterium* containing a plasmid encoding PLS linked to a C-terminal GFP and ETR1 with a C-terminal HA tag was infiltrated into *Nicotiana benthamiana* leaves for transient expression. After 3 d, interaction was confirmed by western blotting after Co-IP with either anti-GFP beads (showing PLS pulls down ETR1) or anti-HA beads (showing ETR1 pulls down PLS) (Fig. 3a). GFP-only controls did not show binding with ETR1, demonstrating the interaction is dependent on the presence of the PLS peptide.

The addition of 0.5 μM copper sulphate to the protein extract used for Co-IP experiments stabilized the PLS-ETR1 interaction. The presence of copper ions resulted in almost 3-fold more PLS:GFP detected upon pulldowns with ETR1-HA, or conversely of ETR1-HA pulled down with PLS-GFP, compared to the same assay in the presence of the metal chelator 2 mM EDTA

(Fig. 3a, b).

To investigate the specificity of PLS binding, synthetic full length PLS peptide PLS(FL) was introduced into the infiltrated *N. benthamiana* leaves 30 min before the tissue was harvested. The addition of 25 nM synthetic PLS caused a ca. 80% reduction in PLS-GFP binding to ETR1-HA (Fig. 3c, d), suggesting that the synthetic PLS peptide competes for ETR1 binding, and showing the specificity of PLS for ETR1. Interestingly, the anti-GFP beads bound two sizes of PLS-GFP protein (Fig. 3e), both of which were larger than a GFP-only control, suggesting that the PLS peptide undergoes cleavage, a change in conformation, post-translational modification or incomplete reduction of Cys residues on some PLS. When using ETR1-HA to pull down PLS-GFP, only the larger peptide was present (Fig. 3e, f), suggesting that ETR1 binds the full length PLS peptide, but that PLS may be modified after ETR1 binding.

To pinpoint the interaction site at the receptor in more detail, binding studies were performed with purified receptor variants and PLS by microscale thermophoresis (MST; Fig. 3g). Binding of PLS was observed only with receptor variants containing the N-terminal transmembrane domain (TMD). In contrast, no binding was detected with ETR1 lacking this domain ($ETR1^{306-738}$). The TMD harbors the ethylene and copper binding region (*22*).

PLS binds Cu(I) and forms protein adducts with copper chaperones ATX and CCH and with RAN1

Cysteine residues are common metal-ligand binding residues in low molecular weight copper-handling peptides, and predictions of PLS structure suggests a single α-helix plus unstructured region with two cysteines ($CX_{10}C$ arrangement where X is any amino acid), with some analogy to copper-metallochaperones such as Cox17 or other CX_9C twin proteins (*23*). In view of both structural considerations and the copper-dependency of ETR1 we determined whether the two cysteine residues (C6 and C17) in PLS play a functional role, such as in copper binding. A mutated *Arabidopsis* full-length peptide in which both cysteines were replaced with serine, PLS(FL C6S, C17S), was non-functional in root feeding assays (Fig. 4a), indicating the importance of the cysteine residues for biological activity. To determine a possible role for PLS in binding Cu(I), we first grew *pls* mutants and wildtype seedlings in the presence of the copper chelator bathocuproine disulphonic acid (BCS), which is often used to deplete copper but notably solubilises and stabilises Cu(I). Treatment of *pls* and wildtype seedlings with 10 µM and 50 µM BCS led to an increased primary root length of both genotypes, while 100 µM BCS led to significantly enhanced root growth in the *pls* mutant compared with wildtype (Fig. 4b); and rescue of the overexpression of ethylene-responsive genes (Fig. S5; *19*). This suggests that the availability of Cu(I) is growth-limiting in the *pls* mutant through abnormal ethylene perception.

Bicinchoninic acid (BCA) is a chromophore that binds Cu(I) (*24*) (Fig. 4c and S6). Titration experiments show that synthetic PLS(FL) withholds Cu(I) from BCA (Fig. S7), but the mutant PLS (FL C6S, C17S) does not (Fig. S8). Attempts to determine the stoichiometry and affinity for Cu(I) were confounded by precipitation of the synthetic peptide, whereas PLS fusion to maltose binding protein (MBP-PLS) retained solubility when titrated with Cu(I) ions under strictly anaerobic conditions. MBP-PLS (14 µM) withholds ca. 7 µM Cu(I) from BCA, indicative of a 2:1 PLS:Cu(I) stoichiometry, and tight binding is cysteine-dependent (Fig. 4d). A β_2 affinity of 3.79 (±1.5) $x10^{19}$ M^{-2} was determined by competition against an excess of BCA, and the fit significantly departs from simulations 10x tighter or weaker (Fig. 4e, Fig. S9).

Metal binding in biology is challenging to predict because the formation of metal-protein complexes is a combined function of metal affinity for a given protein and metal availability, which would need to be known for Cu(I) in the *Arabidopsis* cytosol in the case of PLS (Fig. 2p). Cu(I) occupancy of the cytosolic copper chaperone ANTIOXIDANT PROTEIN 1 (ATX1) tracks

with fluctuations in available cytosolic Cu(I) such that its affinity approximates to the mid-point of the range of Cu(I) availabilities within this eukaryotic compartment (*25, 26*). *Arabidopsis* ATX1 was therefore expressed and purified to determine a 1:1 ATX1:Cu(I) stoichiometry and affinity $K_{D\ Cu(I)}$ of 5.47 (±0.6) x10^{-18} M (Fig. 4f inset, Fig. S10). Figure 4f (main panel) reveals that the cytosolic concentration of PLS would need to exceed (improbable) millimolar concentrations for Cu(I)-dependent homodimers to form at this cytosolic Cu(I) availability (mathematical models and equations shown in Supplementary text). It is thus unlikely that the Cu(I):PLS_2 complex alone delivers Cu(I) to interacting cuproprotein ETR1. Cu(I)-dependent PLS heterodimeric adducts are the more likely functional species.

Together these results suggest a model in which PLS is involved in the RAN1-dependent maturation of Cu(I)ETR1 at the ER. To investigate possible interaction between PLS and RAN1, PLS was titrated to fluorescently labelled RAN1 and RAN1 truncation mutants. RAN1, NterRAN1 and CterRAN1 were purified and labelled as described (*27*). NterRAN1 is a truncation containing only the two N-terminal metal-binding-domains, whereas CterRAN1 is a construct lacking this region. Using Microscale Thermophoresis, direct interaction was observed between PLS and RAN1. Dissociation constants indicate that PLS interacts predominantly with the N-terminal metal-binding-domains, but only weakly with the C-terminal region (Fig. 4g). Moreover, the soluble copper chaperones ATX1 and CCH also interact with PLS. Titration experiments were carried out with fluorescently labelled copper chaperones ATX1, CCH and CCHΔ, a mutant lacking the plant specific C-terminal extension. PLS interacts with these soluble copper chaperones at similar affinity as obtained for RAN1 (Fig. 4h). Of relevance here is the observation that ATX1 interacts directly with RAN1 to deliver copper at the ER (*28*). Cu(I)-dependent PLS heterodimeric adducts may therefore modulate multiple cuproproteins in the Cu(I)ETR1 maturation pathway.

The formation of PLS adducts with otherwise unsaturated copper coordination spheres, can inhibit the formation of aberrant copper-bridged complexes during metalation or during re-organisation of copper sites. This can, in turn, influence the rate of holo-ETR1 maturation, plus potentially the rates of ETR1 deactivation and reactivation. In this model, a down-regulation of *PLS* or loss-of-function mutation of the *PLS* gene leads to a depletion of correctly coordinated Cu(I) at the receptor through reduced intermediate PLS heterodimer adduct formation, in turn leading to a non-functional receptor that cannot activate CTR1, with a consequent activation of ethylene signaling, similar to *ran1* or *etr1* loss-of-function mutants, and/or through the effect of ethylene on reducing *PLS* expression (Figs. S11, S12). Overexpression of PLS phenocopies the ethylene-insensitive *etr1-1* gain-of-function mutant (*18*), presumably by a conformational change in the receptor on binding, to promote a functional interaction with CTR1 and suppressing ethylene responses. The PLS complex may be removed from ETR1 by dissociation of a PLS-ETR1-RAN1-chaperone complex following ligand-exchange, and/or modulated by PLS modification or cleavage. It is speculated that similar PLS-dependent events may also be required to re-set the receptor, perhaps following changes in the copper coordination sphere coincident with gain or loss of cation-π bonds between copper and ethylene. Hormonal regulation of *PLS* expression forms a signaling network to regulate ethylene responses and root growth with other hormones, such as by its activation to suppress growth-inhibitory ethylene responses in the high auxin environment of the root tip (*29*) (Fig. S12). Future structural studies should reveal more about the PLS-adduct-receptor interaction and role of copper ions in ethylene signal transduction, which represents a new paradigm for the regulation of signaling protein function by metals.

Methods

Plant Material

Seedlings of *Arabidopsis thaliana* ecotype either C24 or Col-0, or *pls* mutants or transgenic *PLS* overexpressers, all from lab stocks, were grown on solid sterile half-strength MS10 medium on 2.5% Phytagel (Sigma-Aldrich) in 90 mm Petri dishes (Sarstedt, Leicester, UK) at 21°C, under a 16 hour photoperiod as described (*17, 18*). *Nicotiana benthamiana* plants (lab stocks) were grown in a controlled environment (21°C, 16 h photoperiod) for transient expression studies in leaf tissue. For hydroponic feeding studies, *Arabidopsis* seedlings were cultured in liquid medium (1 ml/well) in sterile 24-well plates (Sarstedt), essentially as described (*30*). For hormone and peptide assays, one seedling was grown in each well, at 21°C, under a 16 h photoperiod. For peptide feeding experiments, purified freeze-dried peptide was dissolved in DMSO to create a 500 µM stock solution. Peptide stock solution was added to liquid ½ MS10 plant media containing 0.1% DMSO to make a final peptide concentration of 50 or 100 nM (or 10, 25, 50 and 100 nM for dose-dependent assays). For copper treatments, 1 mM $CuSO_4$ solution was filter-sterilized and added to autoclaved liquid ½ MS10 plant media to create final $CuSO_4$ concentrations of 0, 5, 10, 15, 20, 25, 30, 35, 40, 45 and 50 µM. The copper chelator bathocuproine disulphonic acid (BCS) was added to liquid medium to produce final concentrations of 0, 10, 50, 100, 250 and 500 µM. Seedlings were scanned to create a digital image and root lengths of seedlings were measured using ImageJ. Statistical analysis was performed using the Real Statistics Resource Pack software (Release 3.8, www.real-statistics.com) in Excel (Microsoft).

Peptide Synthesis

Peptides were either obtained from Cambridge Research Biochemicals (Billingham, UK) or synthesized in the laboratory by Fmoc solid phase peptide synthesis (SPPS) on a CEM Liberty1 single-channel peptide synthesiser equipped with a Discover microwave unit. Reactions were performed in a 30 ml PTFE reaction vessel with microwave heating and agitation by bubbling nitrogen. Peptide synthesis was carried out using 2-chlorotrityl chloride resin (0.122 mmol g^{-1}, Novabiochem) using Fmoc-protected amino acids. The first amino acid residue at the C-terminus (histidine) was coupled manually by mixing 76 mg (1 eq.) Fmoc-His(Trt)-OH, 0.09 ml (4 eq.) *N,N*-diisopropylethylamine (DIPEA), 1 ml dichloromethane (DCM) and 1 ml dimethylformamide (DMF) until the amino acid powder had dissolved. The mixture was added to 0.1 mmol resin and stirred gently for 120 minutes at room temperature. Resin was washed with 3x DCM/MeOH/DIPEA (17:2:1), 3x DCM, 2x DMF and 2x DCM. Amino acid coupling reactions were performed using Fmoc-protected amino acids present in a 5-fold excess (2 M concentration), HOBt (0.5 M HOBt in DMF, used at the activator position) and DIC (0.8 M in DMSO, used at the activator base position). For double and triple couplings the reaction vessel was drained after each coupling cycle and fresh reagents were added. Before each coupling, a room temperature preactivation period of 1 to 2 hours was used. Microwave-assisted couplings were performed for 10 minutes at 75°C at 25W power. Cys and His residues were coupled at low temperature (10 minutes at room temperature followed by 10 minutes at 50°C, 25W). Arg residues were double coupled, firstly by 45 minutes at room temperature plus 5 minutes at 75°C (25W), and second by the standard microwave conditions above. Fmoc group removal was carried out by two piperidine solution treatments (20% piperidine in DMF) in succession: 5 minutes then 10 minutes. Peptide cleavage from resin was carried out in 3 ml 95% TFA in dH_2O/TIPS (2.85 ml TFA, 0.15 ml dH_2O, 0.15 ml triisopropylsilane). Peptide was dissolved in water

with a small volume of MeCN and lyophilized to produce a powder using a Christ ALPHA 1-2 LD_{plus} freeze dryer.

Preparative High-Performance Liquid Chromatography (HPLC)

Peptide products were analysed and purified by HPLC at 280 nm. 25-50 mg of freeze-dried peptide sample was dissolved in 1 ml 1:1 H_2O:MeCN and injected onto a Speck and Burke Analytical C18 Column (5.0 µm, 10.0 x 250 mm) attached to a PerkinElmer (Massachusetts, USA) Series 200 LC Pump and 785A UV/Vis Detector. Separation was achieved by gradient elution of 10-80% solvent B (solvent A = 0.08% TFA in water; solvent B = 0.08% TFA in ACN) over 60 minutes, followed by 80-100% B over 10 minutes, with a flow rate of 2 ml/min. Selected peptide fractions were lyophilized and a mass assigned using MALDI-TOF MS. Peptide sequences were identified using MALDI-TOF MS, using an Autoflex II ToF/ToF mass spectrometer (Bruker Daltonik GmBH, Germany) equipped with a 337 nm nitrogen laser. MS data was processed using FlexAnalysis 2.0 (Bruker Daltonik GmBH).

Imaging

CSLM images were obtained by a Leica SP5 TCS confocal microscope using 40X and 63X oil immersion lenses. For propidium iodide staining, whole *Arabidopsis* seedlings were incubated in 10 mg/l propidium iodide solution for 90 s. *pPLS::PLS:GFP, pPLS::GFP* and *p35S::GFP* seedlings were grown for 7 d on Phytagel ½ MS10 medium before ca. 25 mm of the root tip was removed and mounted in dH_2O on a microscope slide, and a 1.5 mm cover slip was placed on top prior to imaging. The ER marker p35S::RFP:HDEL (*20*) (kindly provided by Dr. Pengwei Wang, Durham University), and the trans-Golgi apparatus marker *pFGC-ST:mCherry* (obtained from Nottingham Arabidopsis Stock Centre, www.arabidopsis.info) were introduced into *pPLS::PLS:GFP* plants by the floral dip method of transformation (*31*) using *A. tumefaciens* GV3 101. ER was also localized using ER Tracker™ Red (Life Technologies). Seven day-old seedlings were stained for 30 min in the dark in liquid ½ MS10 media containing 1 µM ER Tracker™ Red.

RNA Isolation, RNA Sequencing, RT-qPCR

RNA was extracted from 7 day-old seedlings grown on half strength MS10 medium using the Sigma-Aldrich Plant Total RNA Kit (STRN50) and the On-Column DNase I Digestion Set (DNASE10-1SET), essentially as described (*32*). Tissue was ground in liquid nitrogen before incubation in lysis solution containing 2-mercaptoethanol at 65°C for 3 min. Debris was removed by centrifugation and column filtration and RNA was captured onto a binding column using the supplied binding solution. DNA was removed by wash solutions and DNase treatment on the column. Purified RNA was eluted using RNAase free water.

The Illumina HiSeq 2500 System was used for RNA sequencing of three biological replicate samples, with libraries prepared using the Illumina TruSeq Stranded Total RNA with Ribo-Zero Plant Sample Preparation kit (RS-122-2401), essentially as described (*32*). Ribosomal RNA (rRNA) was removed and purified RNA was quality checked using a TapeStation 2200 (Agilent Technology) with High Sensitivity RNA ScreenTape (5067-5579). mRNA was fragmented into 120-200 bp sequences with a median size of 150 bp, and used as template to synthesize first strand cDNA using reverse transcriptase and random primers, followed by second strand cDNA synthesis with DNA Polymerase I and RNase H. Newly synthesized cDNA had a single adenine base added with ligation of adaptors, before being purified and amplified by PCR to make the final library. Library quality control was carried out again using a TapeStation with D1000 ScreenTape (catalog number 5067-5582). RNA-seq data were processed and aligned against the

TAIR10 (EnsemblePlants) genome using TopHat and indexed with Samtools. DeSeq determined differential expression. A padj-value of ≤ 0.05 and a $\log_2$fold change ($\log_2$FC) of ≥ 0.5 were selected to identify differentially expressed genes (DEGs). RNA-seq data are deposited in the Dryad Digital Repository (*19*).

For RT-qPCR, RNA was extracted from 7 day-old seedlings (3 biological replicates, 20 mg of tissue) as described (*32*). Total mRNA was extracted using Dynabeads®mRNA DIRECT™kit with Oligo(dT)$_{25}$ labelled magnetic beads. cDNA was prepared using a SuperScript®IV First-Strand synthesis system. Samples were checked for the presence of genomic DNA by PCR with *ACTIN2* primers ACT2 forward and reverse. Primer sequences were determined using Primer-BLAST (https://www.ncbi.nlm.nih.gov/tools/primer-blast/). Primers are listed in Table S2.

Protein-protein interaction studies

Yeast 2-hybrid

The GAL4 two-hybrid phagemid vector system was used to detect protein-protein interactions *in vivo* in yeast, using the reporter genes β-galactosidase *(lacZ)* and histidine (*HIS3*) in the YRG-2 yeast strain, essentially as described (*34*). DNA that encodes the target (ETR1) and bait (PLS) was inserted into the pAD-GAL4-2.1 A and pBD-GAL4 Cam phagemid vectors respectively and expressed as hybrid protein. The hybrid proteins were then assayed for protein-protein interaction.

DNA encoding the target and bait proteins were prepared by PCR amplification using primer designed the specifically for the DNA encoding the target (ETR1) and bait (PLS). Each set of primer contained specific endonucleases on the ends of primer corresponding to the endonucleases in the MCS of pAD-GAL4-2.1 A and pBD-GAL4 Cam phagemid vectors. The DNA construct of the target (ETR1) and bait (PLS) with specific restriction sites on the ends was then transformed into the TOPO 2.1 vector to check the sequence of the amplified DNA by sequencing with M13 forward (CTG GCC GTC GTT TTA C) and M13 reverse (CAG GAA ACA GCT ATG AC). The two vectors, pAD-GAL4-2.1 and pBD-GAL4 Cam were digested using specific restriction endonucleases and dephosphorylated prior to ligating the insert DNA. The DNA encoding the target (ETR1) and bait (PLS) was then ligated into the same reading frame as the GAL4 AD of the pAD-GAL4-2.1 phagemid vector and the GAL4 BD of the pBD-GAL4 Cam phagemid vector.

The following primers were used for PCR amplification:

ETR1:

Forward primer GAA TCC ATG GAA GTC TGC AAT TGT A (Eco RI on 5’ end)

Reverse primer GTC GAC TTA CAT GCC CTC GTA CA (Sal I on 5’end)

PLS:

Forward primer CTG GAG ATG AAA CCC AGA CTT TGT (Xho I on 5’ end)

Reverse primer GTC GAC ATG GAT TTT AAA AAG TTT (Sal I on 5’ end)

The pGAL4 control plasmid was used alone to verify that induction of the *lacZ* and *HIS3* genes has occurred and that the gene products are detectable in the assay used. The pLamin C control plasmid was used in pairwise combination with the pAD-WT control plasmid or with the pAD-MUT control plasmid to verify that the *lacZ* and *HIS3* genes are not induced as the protein expressed by each of these pairs do not interact *in vivo*.

The control plasmids were transformed into the YRG-2 strain prior to the initial transformation of the bait and the target plasmids. The control plasmids were used separately or in pairwise combination in the transformation of the YRG-2 yeast strain. The yeast competent cells were cotransformed with the bait and target plasmids by sequential transformation. First, yeast were

transformed with the bait plasmid and assayed for expression of reporter genes. Second, yeast competent cells containing the bait were prepared and transformed with the target plasmid.

Bimolecular fluorescence complementation analysis (BiFC)

BiFC was carried out essentially as described previously (*35*). Full-length *Arabidopsis* ETR1 and PLS cDNA sequences were cloned respectively into the vectors pDH51-GWYFPn (AM779183, to form ETR1-YFPn) and pDH51-GW-YFPc (AM779184, to form PLS-YFPc), and the CTR1 cDNA was cloned into pDH51-GW-YFPc (CTR1c), as a control for ETR1 interactions. Intact YFP plasmid was also used as a positive control and YFPc alone was used as a negative control as described previously (*34*). Plasmids were kindly provided by Prof. Don Grierson, University of Nottingham. Transient expression studies following microprojectile bombardment on onion cells. Plasmids were adhered to gold particles to make gold-coated cartridges. 5-10 of these cartridges were used for bombarding onion peel cells. Agar plates containing bombarded onion peels were incubated for 8 hours in dark and then a 1 cm section of the peel was stained with propidium iodide (10 mg/ml) for 1 min and viewed under confocal microscope. Experiments were repeated at least three times.

Co-immunoprecipitation

To investigate the interaction between the PLS peptide and the ethylene receptor ETR1, two DNA constructs were created by Gateway cloning. The 105-nucleotide *PLS* gene (without the stop codon) was inserted into the pEarlyGate103 (pEG103) destination vector, containing the *p35S* promoter and a C-terminal GFP tag, producing a vector containing the *p35S::PLS:GFP* DNA. The ETR1 cDNA was inserted into the pEarlyGate301 (pEG301) vector to create a *p35S::ETR1:HA* construct, producing an ETR1 protein with a C-terminal HA tag.

Infiltration into *Nicotiana benthamiana*

The transient expression of constructs in *Nicotiana benthamiana* (tobacco) leaves was based on a previously published method (*36*). Experiments were replicated up to 5 times. Competent *Agrobacterium tumefaciens* GV3101 cells were transformed with the desired plasmid containing the gene of interest. Individual colonies were used to inoculate liquid LB cultures containing 25 µg/ml gentamicin, 50 µg/ml rifampicin and the specific antibiotic required to select for the desired plasmid. The liquid cultures were grown at 28°C for 14-16 h with shaking at 220 rpm. Additionally, liquid cultures of GV3101 containing the p19 protein that is encoded by the tomato bushy plant virus were also prepared in order to suppress post-transcriptional gene silencing (*36*). The overnight cultures were grown until an OD_{600} of approximately 0.6 was reached, and then centrifuged at 3000 x *g* for 5 min. These cells were then twice washed with 10 ml of an infiltration buffer containing 10 mM $MgCl_2.6H_20$, resuspended in 1 ml of the same solution and subsequently incubated at room temperature for 3-5 h. Prior to infiltration, each construct was mixed with p19 and infiltration buffer in a 1:1.2:1.8 ratio.

Several small cuts were made with a scalpel on the abaxial surface of the *N. benthamiana* leaves, and were subsequently injected with each of the constructs using a syringe. The plants were approximately 7 to 10 weeks old; the chosen leaves were healthy and of length 3-6 cm, and 3 to 4 leaves were infiltrated with each construct.

Protein extraction and PLS/ETR1 co-immunoprecipitation

Total protein was extracted from the infiltrated leaves of *N. benthamiana* plants 3 d after infiltration for co-immunoprecipitation (Co-IP/pull-down) experiments to investigate the interaction between PLS and ETR1 proteins.

1.5 g of leaf tissue was harvested from each *A. tumefaciens* construct infiltration event, frozen with liquid nitrogen and ground gently using a mortar and pestle. For competition assays, 5 nM or 25 nM full-length PLS peptide was also infiltrated in the presence of 50 µM MG-132 (a proteasome inhibitor) 30 min prior to tissue freezing. The homogenate was transferred to a pre-cooled microcentrifuge tube. 2 ml of extraction buffer was added (20 mM sodium phosphate pH 7.4, 100 mM NaCl, 80 mM KCl, 1% glycerol, 0.1 % Triton, 10 mM DTT, plus 1 mini protease inhibitor cocktail tablet, Roche, Switzerland) per 20 ml of extraction buffer, and the extra addition of either 2 mM EDTA or 0.5 µM $CuSO_4$ for binding studies), and the solution was ground further and vortexed until the homogenate was smooth. The solution was centrifuged for 12 min at 14000 x *g*, 4°C.

ChromoTek (Planegg, Germany) anti-GFP beads were used to immunoprecipitate the PLS-GFP protein, and Sigma-Aldrich (St. Louis, USA) anti-HA beads for the HA-tagged ETR1. 25 µl bead slurry was resuspended in 500 µl ice-cold dilution buffer (20 mM sodium phosphate pH 7.4, 100 mM NaCl, 80 mM KCl, 1% glycerol, 0.1 % Triton, 10 mM DTT, plus 1 mini protease inhibitor cocktail tablet) and centrifuged for 2 minutes at 2500 x *g* at 4°C. The supernatant was discarded and the beads were washed twice more with 500 µl ice-cold dilution buffer.

The supernatant from the protein sample extraction from *N. benthamiana* plants was mixed with 50 µl GFP beads or HA beads and incubated for 30 minutes at 4°C, mixing every 2 minutes. The mixture was centrifuged at 2500 x *g* for 2 min at 4°C, washed twice with 500 µl ice-cold dilution buffer, and the beads were transferred to a new microcentrifuge tube. The target protein was eluted with the addition of 100 µl 2x SDS sample buffer (120 mM Tris pH 6.8, 50 mM 4% (w/v) SDS, 20% (v/v) glycerol) and the sample was boiled for 10 minutes at 95°C to dissociate immunocomplexes from the beads. The mixture was centrifuged for at 2500 x *g* for 2 minutes at 4°C to separate the beads, and the supernatant was transferred to a new microcentrifuge tube. The supernatant was used in SDS-PAGE analysis.

Sodium Dodecyl Sulphate Polyacrylamide Gel Electrophoresis (SDS-PAGE)

SDS-PAGE was used to separate protein fragments. The complexed proteins from the pull-down assay were analysed on 10-12% acrylamide gels.

Firstly, the resolving gel was prepared by adding the chosen amount of acrylamide (ProtoGel, 30% (w/v) acrylamide, 0.8% (w/v) bisacrylamide solution, National Diagnostics) to the resolving buffer (0.1% (w/v) SDS, 375 mM Tris, polymerized via the addition of 0.1% (v/v) ammonium persulphate solution (APS) and finally set by the addition of 1.4 µl/ml TEMED (NNN'N'-tetramethylethylenediamine). The stacking gel was then prepared again by adding the appropriate amount of acrylamide to the stacking buffer (consisting of 0.1% w/v SDS, 125 mM Tris). Polymerization was activated by adding 0.1% (v/v) APS and set using 4 µl/ml TEMED.

SDS-PAGE gels were run in a tank containing an electrode buffer (25 mM Tris, 0.1% (v/v) glycerol, 190 mM glycine, diluted 1:10 with dH2O) at 90 V for approximately 90 min. 6 µl PageRuler™ Plus Prestained Protein Ladder, 10 to 250 kDa (ThermoFisher Scientific) was loaded as a protein size marker, displaying coloured bands at 10, 15, 25, 35, 55 70, 100, 130 and 250 kDa.

Western Blotting

Following electrophoresis, the SDS gels were first washed in 1x transfer buffer (0.04% (w/v) SDS, 20% (v/v) methanol, 38 mM glycine, 48 mM Tris) for 5 minutes. The proteins were then transferred overnight onto nitrocellulose membranes (Whatman, GE Healthcare Life Sciences, Buckinghamshire, UK) in a 1 litre tank containing transfer buffer at 30 V.

The nitrocellulose membranes were incubated in milk buffer (5% (w/v) dried skimmed milk powder (Tesco, Durham, UK), 150 mM NaCl, 10 mM Tris, 0.1% (v/v) Tween 20, pH 7.4) for 20 min to block non-specific protein binding. Following this treatment, the membranes were incubated with primary antibody for 2.5 h (GFP, Abcam, Cambridge, UK: rabbit, 1:10000; HA [Roche], rat, 1:3000). Excess primary antibody was then removed by washing three times in 2x TBST (150 mM NaCl, 10 mM Tris, 0.1% (v/v) Tween 20, pH 7.4) for 2 m, 5 min and 10 min, and subsequently incubated for 1 h with the ECL peroxidase-labelled anti-rabbit or anti-rat IgG secondary antibody, diluted 1:20000 in TBST. Excess secondary antibody was removed again by washing three times in 1x TBST, as with the primary antibody. In order to visualize the probed blot, the membrane was incubated with ECL Western Blotting Detection Reagent immediately prior to imaging. The horseradish peroxidase conjugated to the secondary antibody was detected by using X-ray film, which was subsequently developed in a dark room.

Estimation of synthetic PLS concentration

Freeze-dried synthetic PLS peptide (Cambridge Research Biochemicals, Billingham) was dissolved in DMSO. An aliquot was added to aqueous buffer (10 mM HEPES pH7, 20 mM NaCl, 80 mM KCl) and absorbance at 280 nm was recorded. Concentration was estimated from the absorbance and the ProtParam estimated extinction coefficient of 2,980 M^{-1} cm^{-1}. Concurrent with this a sample was submitted for quantitative amino acid analysis (Abingdon Health Laboratory Services). From this analysis a conversion factor of 2.27 was generated, which was applied to concentrations determined by A280 nm.

ATX1 purification

E. coli BL21(DE3) containing pETatx1 was used to overexpress the wildtype *ATX1* gene from *Arabidopsis thaliana* (optimised for expression in *E. coli*, Novoprolabs). Harvested cells were collected and frozen at -20 ºC overnight then defrosted, resuspended in 20 mM HEPES (pH 7.0), 10 mM EDTA, 100 mM NaCl, 10 mM DTT. Cells were sonicated (Bandelin Sonoplus), supernatant separated by size exclusion chromatography (GE Healthcare, HiLoad 26.600 Superdex 75 pg) metal-free buffer lacking EDTA. Fractions containing ATX1 were incubated overnight and pooled before transfer into an anaerobic chamber (Belle Technology) via desalting column where reductant was removed. ATX1 was quantified by combination of Bradford assay and Ellman's reagent to ensure the fully reduced state of the protein. Samples were also analysed for metal content by ICP-MS to ensure > 95% apo-ATX1.

MBP-PLS/mutant purification

A fusion of PLS to MBP was created using the NEBExpress MBP Fusion and Purification System. Two complementary oligonucleotide primers encoding PLS (optimised for expression in *E. coli*) were annealed and inserted into the pMal-c5x plasmid at XmnI and SalI insertion sites.

The three mutants MBP-PLS(C6S), MBP-PLS(C17S) and MBP-PLS(C6S/C17S) were created by site-directed mutagenesis (QuikChange II, Agilent). *E. coli* NEB Express containing the pMal plasmid with the correct MBP-PLS mutant was used to overexpress each protein. Harvested cells were resuspended in 20 mM Tris-HCl (pH 7.4), 200 mM NaCl, 1 mM EDTA and frozen at -20 ºC overnight. Cells were defrosted in cold H_2O, sonicated, purified by ammonium sulphate precipitation (where MBP-PLS precipitates >60% saturation), separated on MBP-trap (GE Healthcare) and eluted using buffer containing 10 mM maltose. MBP-PLS-containing fractions were pooled and concentrated using centrifugal concentrator (Corning, Spin-X UF 30 KDa) and buffer exchanged by desalting column into metal-free 20 mM HEPES (pH 7.0), 50 mM NaCl buffer in an anaerobic chamber (Belle Technology). Mutants containing thiols were quantified

Ellman's assay and MBP-PLS(C6S/C17S), which lacks all thiols, was quantified by Bradford assay alone. Samples were also analysed for metal content by ICP-MS to ensure >95% apo-protein.

Anaerobic spectroscopic analysis of Cu(I) complexes

All Cu(I) titration experiments were carried out in an anaerobic chamber (Belle Technology) using metal-free CHELEX-treated, degassed buffers. For experiments titrating Cu(I), aqueous $CuSO_4$ stock was quantified in advance by ICP-MS and diluted to working concentrations. The reductant NH_2OH was included at final concentration of 1 mM to retain Cu(I) in its reduced state. Proteins were diluted in buffer to the final concentration specified in each titration in air-tight quartz cuvettes (Helma), and after addition of probe to the concentration specified, titrated with $CuSO_4$. After each addition, solutions were thoroughly mixed and absorbance spectra recorded using a Lambda 35 UV/Vis spectrophotometer (Perkin Elmer). Titration isotherm data was fitted using simulated affinity curves using Dynafit (*37*).

Interaction studies of PLS with copper transporter ETR1 by Microscale Thermophoresis

Fluorescently labelled ETR1 truncation mutants were added to a dilution series of PLS in 50 mM HEPES, 150 mM NaCl, 0.015 % (wv) FosCholine 16 (pH 7.6) or 50 mM Tris, 300 mM NaCl, 0.015 % (w/v) FosCholine 16 (pH 7.6). Dissociation constants were calculated using GraphPad Prism 5.

Determination of dissociation constants for the PLS-ETR1 interaction

Full-length ETR1 and truncation mutants were purified and labelled as described in (*38*). 94 µM PLS were diluted serially in 50 mM Tris and 300 mM NaCl (pH 7.6). Fluorescently labelled receptor was added at a final concentration of 50 nM. Thermophoretic behaviour was measured in premium capillaries at 50 % LED and 50 % MST power. In case of a binding event, data were fitted using GraphPad Prism 5.

Interaction studies of PLS with copper transporter RAN1 and copper chaperones by Microscale Thermophoresis

PLS was titrated to fluorescently labelled RAN1 and RAN1 truncation mutants. RAN1, NterRAN1 and CterRAN1 were purified and labelled as described in (*27*). NterRAN1 is a truncation containing only of two N-terminal metal-binding-domains, whereas CterRAN1 is a construct lacking this region. Direct interaction between PLS and RAN1 was observed using Microscale Thermophoresis. Dissociation constants indicate that PLS interacts predominantly with the N-terminal metal-binding-domains, but only weakly with the C-terminal region. Dissociation constants were determined using GraphPad Prism 5. Titration experiments were also carried out with fluorescently labelled copper chaperones ATX, CCH and CCHΔ, a mutant lacking the plant specific C-terminal extension. Proteins were purified and labelled as described (*27*).

Ratiometric analysis of roGFP2 fusion proteins

N- and C-terminal roGFP2 fusion proteins of PLS were generated by Gateway cloning. Infiltration and transient expression of roGFP2 fusions and control proteins were carried out as described in (*39*). Image acquisition and data analysis were carried out as described in (*27*). A minimum of 10 leaf optical sections were imaged and used for ratiometric analysis of the redox sensitive excitation properties of roGFP2.

Statistical methods

For gene expression analysis and growth assays, a minimum of three biological replicates was used - see Supplementary Materials, Figure legends, Supplementary Table S1, expression data on Dryad (*19*). For protein-protein interaction and protein localization studies, assays were carried out independently between 2 and 10 times (Figs. 2, 3 legends). At least three biological replicates were used for plant growth assays, RNA-seq and gene expression (RT-qPCR) experiments, metal binding assays (Fig. 4). Normalised values from at least three biological replicates were then used for one- or two-way analysis of variance (ANOVA) where appropriate and indicated in relevant Figure legends. Error bars are defined in Figure legends, where relevant.

References

1. Johnson, P.R., Ecker J.R. The ethylene gas signal transduction pathway: A molecular perspective. *Ann. Rev. Genet.* ***32***, 227-254 (1998).

2. Chang, C., Kwok, S.F., Bleecker, A.B., Meyerowitz, E.M. Arabidopsis ethylene-response gene *ETR1* - similarity of product to 2-component regulators. *Science* **262**, 539-544 (1993).

3. Hua, J., Chang, C., Sun, Q., Meyerowitz, E.M. Ethylene insensitivity conferred by Arabidopsis *ERS* gene. *Science* **269**, 1712-1714 (1995).

4. Hua, J., Sakai, H., Nourizadeh, S., Chen, Q.G., Bleecker, A.B., Ecker, J.R., Meyerowitz, E.M. EIN4 and ERS2 are members of the putative ethylene receptor gene family in Arabidopsis. *Plant Cell* **10**, 1321-1332 (1998).

5. Sakai, H., Hua, J., Chen, Q.G., Chang, C., Medrano, L.J., Bleecker, A.B., Meyerowitz, E.M. *ETR2* is an *ETR1*-like gene involved in ethylene signaling in *Arabidopsis*. *Proc. Natl. Acad. Sci. USA* **95**, 5812-5817 (1998).

6. Chen, Y.F., Randlett, M.D., Findell, J.L., Schaller, G.E. Localization of the ethylene receptor ETR1 to the endoplasmic reticulum of Arabidopsis. *J. Biol. Chem*. **277**, 19861-19866 (2002).

7. Grefen, C., Staedele, K., Ruzicka, K., Obrdlik, P., Harter, K., Horak, J. Subcellular localization and in vivo interactions of the *Arabidopsis thaliana* ethylene receptor family members. *Molec. Plant* **1**, 308-320 (2008).

8. Schaller, G.E., Ladd, A.N., Lanahan, M.B., Spanbauer, J.M., Bleecker, A.B. The ethylene response mediator ETR1 from Arabidopsis forms a disulfide-linked dimer. *J. Biol. Chem*. **270**, 12526-12530 (1995).

9. Hall, A.E., Findell, J.L., Schaller, G.E., Sisler, E.C., Bleecker, A.B. Ethylene perception by the ERS1 protein in Arabidopsis. *Plant Physiol.* **123**, 1449-1457 (2000).

10. Rodriguez, F.I., Esch, J.J., Hall, A.E., Binder, B.M., Schaller, G.E., Bleecker, A.B. A copper cofactor for the ethylene receptor ETR1 from Arabidopsis. *Science* **283**, 996-998 (1999).

11. McDaniel, B.K., Binder, B.M. ETHYLENE RECEPTOR 1 (ETR1) is sufficient and has the predominant role in mediating inhibition of ethylene responses by silver in *Arabidopsis thaliana*. *J. Biol. Chem.* **287**, 26094-26103 (2012).

12. Chang, C.R. Ethylene signaling: the MAPK module has finally landed. *Trends Plant Sci.* **8**, 365-368 (2003).

13. Gao, Z.Y., Chen, Y.-F., Randlett, M.D., Zhao, X.-C., Findell, J.L., Kieber, J.J., Schaller, G.E. Localization of the Raf-like kinase CTR1 to the endoplasmic reticulum of Arabidopsis through participation in ethylene receptor signaling complexes. *J. Biol. Chem*. **278**, 34725-34732 (2003).

14. Hirayama, T., Kieber, J.J., Hirayama, N., Kogan, M., Guzman, P., Nourizadek, S., Alonso, J.M., Dailey, W.P., Dancis, A., Ecker, J.R. RESPONSIVE-TO-ANTAGONIST1, a Menkes/Wilson disease-related copper transporter, is required for ethylene signaling in Arabidopsis. *Cell* **97**, 383-393 (1999).

15. Binder, B.M., Rodriguez, F.I., Bleecker, A.B. The copper transporter RAN1 is essential for biogenesis of ethylene receptors in Arabidopsis. *J. Biol. Chem*. **285**, 37263-37270 (2010).

16. Qu, X., Hall, B.P., Gao, Z.Y., Schaller, G.E. A strong constitutive ethylene-response phenotype conferred on Arabidopsis plants containing null mutations in the ethylene receptors *ETR1* and *ERS1*. *BMC Plant Biol*. **7**, 3 (2007).

17. Casson, S.A., Chilley, P.M., Topping, J.F., Evans, I.M., Souter, M.A., Lindsey, K. The *POLARIS* gene of Arabidopsis encodes a predicted peptide required for correct root growth and leaf vascular patterning. *Plant Cell* **14**, 1705-1721 (2002).

18. Chilley, P.M., Casson, S.A., Tarkowski, P., Hawkins, N., Wang, K.L., Hussey, P.J., Beale, M., Ecker, J.R., Sandberg, G.K., Lindsey, K. The POLARIS peptide of Arabidopsis regulates auxin transport and root growth via effects on ethylene signaling. *Plant Cell* **18**, 3058-3072 (2006).

19. Mudge, A.J., Mehdi, S., Michaels, W., Orosa-Puente, B., Shen, W., Sadanandom, A., Hetherington, F.M., Hoppen, C., Uzun, B., Groth, G., Topping, J.F., Robinson, N.J., Lindsey, K. Data from: A peptide that regulates metalation of the *Arabidopsis* ethylene receptor. *Dryad Digital Repository.* https://doi.org/10.5061/dryad.wpzgmsbss.

20. Lee, H., Sparkes, I., Gattolin, S., Dzimitrowicz, N., Roberts, L.M., Hawes, C., Frigerio, L. An Arabidopsis reticulon and the atlastin homologue *RHD3-like2* act together in shaping the tubular endoplasmic reticulum. *New Phytol.* **197**, 481-489 (2013).

21. Bauer, M., Papenbrock, J. Identification and characterization of single-domain thiosulfate sulfurtransferases from Arabidopsis thaliana. *FEBS Lett*. **532**, 427-431 (2002).

22. Schott-Verdugo, S., Müller, L., Classen, E., Gohlke, H., Groth, G. Structural model of the ETR1 ethylene receptor transmembrane sensor domain. *Sci Rep.* **9,** 8869 (2019).

662 23. Robinson, N.J., Winge, D.R. Copper metallochaperones. *Ann. Rev. Biochem.* **79**, 537-562
663 (2010).
664
665 24. Xiao, Z., Brose, J., Schimo, S., Ackland, S.M., La Fontaine, S., Wedd, A.G. Unification of
666 the copper(I) binding affinities of the metallo-chaperones Atx1, Atox1, and related proteins:
667 detection probes and affinity standards. *J. Biol. Chem.* **286**, 11047-11055 (2011).
668
669 25. Morgan, M.T., Bourassa, D., Harankhedkar, S., McCallum, A.M., Zlatic, S.A. *et al.*
670 Ratiometric two-photon microscopy reveals attomolar copper buffering in normal and Menkes
671 mutant cells. *Proc. Natl. Acad. Sci. USA* **116**, 12167–12172 (2019).
672
673 26. Yu, C.H., Yang, N., Bothe, J., Tonelli, M., Nokhrin, S., Dolgova, N. V., *et al.* The metal
674 chaperone Atox1 regulates the activity of the human copper transporter ATP7B by modulating
675 domain dynamics. *J. Biol. Chem.* **292**, 18169 (2017).
676
677 27. Hoppen, C., Müller, L., Hänsch, S., Uzun, B., Milic, D., Meyer, A.J., Weidtkamp-Peters, S.,
678 Groth, G. Soluble and membrane-bound protein carrier mediate direct copper transport to the
679 ethylene receptor family. *Sci Rep.* **9**, 10715 (2019).
680
681 28. Li, W., Lacey, R.F., Ye, Y., Lu, J., Yeh, K.-C., Xiao, Y., Li, L., Wen, C.-K., Binder, B.M.,
682 Zhao, Y. Triplin, a small molecule, reveals copper ion transport in ethylene signaling from
683 ATX1 to RAN1. *PLOS Genet.* **13**, e1006703.
684
685 29. Liu, J., Mehdi, S., Topping, J., Tarkowski, P., Lindsey, K. Modelling and experimental
686 analysis of hormonal crosstalk in Arabidopsis. *Molec. Systems Biol*. **6**, 373 (2010).
687
688 30. Matsuzaki, Y., Ogawa-Ohnishi, M., Mori, A., Matsubayashi, Y. Secreted peptide signals
689 required for maintenance of root stem cell niche in Arabidopsis. *Science* **329**, 1065-1067 (2010).
690
691 31. Clough, S.J., Bent, A.F. Floral dip: a simplified method for *Agrobacterium*-mediated
692 transformation of *Arabidopsis thaliana*. *Plant J*. **6**, 735-743 (1998).
693
694 32. Thompson, H.L., Shen, W., Matus, R., Kakkar, M., Jones, C., Dolan, D., Grellscheid, S.,
695 Yang, X., Zhang, N., Mozaffari-Jovin, S., Chen, C., Zhang, X., Topping, J.F., Lindsey, K.
696 MERISTEM-DEFECTIVE regulates the balance between stemness and differentiation in the
697 root meristem through RNA splicing control. *Development* **150**, dev201476.
698
699 33. Love, M.I., Huber, W., Anders, S. Moderated estimation of fold change and dispersion for
700 RNA-seq data with DESeq2. *Genome Biol.* **15**, 550 (2014).
701
702 34. Zhong, S., Lin, Z., Grierson, D. Tomato ethylene receptor-CTR interactions: visualization of
703 NEVER-RIPE interactions with multiple CTRs at the endoplasmic reticulum. *J. Exp. Bot.* **59**,
704 965-972 (2008).
705
706 35. Brandizzi, F., Snapp, E.L., Roberts, A.G., Lippincott-Schwartz, J., Hawes, C. Membrane
707 protein transport between the endoplasmic reticulum and the golgi in tobacco leaves is energy
708 dependent but cytoskeleton independent: Evidence from selective photobleaching. *Plant Cell* **14**,
709 1293-1309 (2002).

36. Voinnet, O., Rivas, S., Mestre, P., Baulcombe, D. An enhanced transient expression system in plants based on suppression of gene silencing by the p19 protein of tomato bushy stunt virus. *Plant J*. **33**, 949-956 (2003).

37. Kuzmič, P. DynaFit—A Software Package for Enzymology. *Meth. Enzymol*. **467**, 247–280 (2009).

38. Milić, D., Dick, M., Mulnaes, D., Pfleger, C., Kinnen, A., Gohlke, H. *et al.*, Recognition motif and mechanism of ripening inhibitory peptides in plant hormone receptor ETR1. *Sci. Rep.* **8**, 1–12 (2018).

39. Brach, T., Soyk, S., Mueller, C., Hinz, G., Hell, R., Brandizzi, F., Meyer, A.J. Non-invasive topology of membrane proteins in the secretory pathway. *Plant J.* **57**, 534-541 (2009).

Acknowledgements: We thank Prof. Steven Cobb (Durham University Department of Chemistry) for advice on peptide synthesis, and Dr. Andrew Foster (Durham University Department of Chemistry) for preliminary peptide-Cu interaction analysis. The authors acknowledge financial support from: UK Biotechnology and Biological Sciences Research Council BB/E006531/1, BBS/B/0773X, BB/J014516/1 (KL), BB/V006002/1, BB/M011186/1 (NJR); Deutsche Forschungsgemeinschaft (German Research Foundation) 267205415 – SFB 1208 project B06 (GG).

Author contributions:
KL and NJR initiated the project. KL, JFT, NJR, AS and GG designed and supervised aspects of the project. AJM, SM, WM, BO-P, WS, FMH, CH and BU carried out the experimental work and prepared the Figures. KL, NJR and GG drafted the early version of the manuscript, and all authors reviewed and edited the manuscript.

Competing interests: Authors declare no competing interests.

Additional information
Supplementary information The online version contains supplementary materials and RNA-seq and root assay data are available at the Dryad Digital Repository (https://doi.org/10.5061/dryad.wpzgmsbss).

Correspondence and requests for materials should be addressed to Keith Lindsey or Nigel Robinson.

Figure Legends
Figure 1. The PLS peptide is required for ethylene control of seedling growth, is structurally and functionally conserved, and complements the *Arabidopsis pls* mutant.
(**a**). Amino acid sequence of the PLS peptide from *Arabidopsis thaliana* with *Camelina sativa* PLS sequence (*C.s* PLS), and synthetic truncations N1, N2, C1 and C2, indicated by horizontal lines. Two cysteine residues are highlighted in bold. (**b**) Wildtype (left) and *pls* mutant (right); bar = 5 mm. (**c**) Expression levels of 24 ethylene-responsive genes in *pls* and *PLS* overexpressing

seedlings, compared to wildtype levels. (**d**) Effect of *Arabidopsis* PLS full length peptide, *A.t.* PLS(FL), and *Camelina* PLS peptide (*C.s.* PLS) on *Arabidopsis* primary root length. Wildtype (C24) and *pls* mutant seedlings were grown hydroponically in the presence (100 nM) or absence of peptide for 10 d. Asterisks: ANOVA, $F_{2, 41} = 6.86$, $p = 0.003$; Tukey's HSD test. (**e**) Effect of PLS full length and truncated peptides on *Arabidopsis* primary root length. Seedlings were grown hydroponically in the presence of 50 nM peptide for 10 d. C1 = C-terminal 14 amino acids, C2 = C-terminal 24 amino acids, N1 = N-terminal 22 amino acids, N2 = N-terminal 9 amino acids, full length PLS = 36 amino acids. Asterisks: ANOVA, $F_{5,112} = 6.13$, $p = 4.65E\text{-}5$). Error bars show ± 1 standard error, n = 14-22.

Figure 2. PLS localizes to the endoplasmic reticulum.
(**a-o**) PLS::PLS:GFP fusion protein (**a, g, j**) colocalizes with endoplasmic reticulum markers ER Tracker (**b, c, c inset**) and RFP:HDEL (**h, i, i inset**), but free GFP does not (**d-f**, **m-o**). PLS:GFP staining is seen also in nuclei (n). PLS::PLS:GFP (**j**) does not co-localize with the *trans*-Golgi markers ST-mCherry SH:GFP (**k, l**). Scale bars = 25 µm (**c, l**), 10 µm (**f, i, o**). (**p**) Ratiometric analysis of roGFP2 fusion constructs transiently expressed in *N. benthamiana*. Comparison of excitation ratios of PLS-roGFP2 and roGFP2-PLS with control constructs (free roGFP, SEC22 fusions) reveals that PLS localizes to the cytosolic side of the ER.

Figure 3. PLS interacts with the ethylene receptor ETR1.
(**a**) Co-immunoprecipitation of PLS:GFP by ETR1:HA (upper panel) in leaves of *Nicotiana benthamiana*, in the presence and absence of 0.5 µM $CuSO_4$ and EDTA (to remove Cu). Lower panel shows presence of ETR1:HA in extracts using anti-HA antibody. (**b**) Densitometric scan of immunoblot. (**c**) Competition assay showing a reduced binding between PLS:GFP and ETR1:HA in the presence of 0, 5 nM or 25 nM PLS peptide, in the presence of 0.5 µM $CuSO_4$ and 50 µM MG-132, a proteasome inhibitor (upper panel). Lower panel shows ETR1:HA in extracts using anti-HA antibody. (**d**) Densitometric scan of immunoblot. (**e**) Co-immunopreciptation of ETR1:HA (upper panel) in leaves of *N. benthamiana*, showing the effect of EDTA (to remove Cu) on interaction between ERT1:HA and PLS:GFP. Lower panel shows presence of ETR1:HA in extracts using anti-HA antibody (**f**) Densitometric scan of immunoblot. α-GFP, anti-GFP antibody; α-HA, anti-HA antibody. (**g**) Microscale thermophoresis binding curves of different ETR1 truncations with PLS. Binding of PLS was observed with full-length ETR1 and all C-terminal truncations but not with $ETR1^{306\text{-}738}$ lacking the N-terminal transmembrane part of the receptor.

Figure 4. PLS binds copper and interacts with RAN1 and copper chaperones.
(**a**) C6S and C17S in PLS are required for function. Seedlings were grown hydroponically for 10 d in the presence (100 nM) or absence of peptide (FL or C6S, C17S). Asterisk: ANOVA, $F_{2, 51} = 9.48$, $p = 3.15E\text{-}4$, Tukey's HSD). Error bars show ± 1 standard error, n = 14-22. Blue bars are C24, red bars are *pls*. (**b**) Effect of exogenous Cu(I) chelator BCS on primary root length of *Arabidopsis* grown hydroponically for 10 d. Asterisks: Student's t test analysis, $p < 0.005$. Error bars show ±1 standard error. (**c**) Absorption of BCA (17.3 µM) titrated with Cu(I) (representative spectrum, n = 2, full dataset Fig S1). (**d**) Binding isotherms ($A_{358\ nm}$) of BCA (10 µM) in the presence/absence (filled/empty symbols, respectively) of 14 µM MBP-PLS (circles) or MBP-PLS mutants (C6S, C17S and C6S/C17S: triangles, diamonds and squares respectively) titrated with Cu(I) (n = 3, ±SD). (**e**) Binding isotherms ($A_{358\ nm}$) of BCA (50 µM) in the presence/absence of 10 µM MBP-PLS (filled/empty symbols, respectively) titrated with Cu(I). Model (solid line) describes Cu(I)-binding as a 2:1 complex, with β_2 affinity of 3.79 (±1.5) $x10^{19}$ M^{-2}. Dotted lines

simulate 10x weaker or tighter affinity (n = 3, ±SD). (**f**) Simulated Cu(I) occupancy (Supplementary Text) as a function of [PLS] using β_2 Cu(I) affinity of 3.79 x10^{19} M^{-2}. Inset, *Arabidopsis* ATX1 (20 μM, filled circles) withholds one Cu(I) equivalent from 20 μM BCA (open circles, BCA-alone) (n = 3, ±SD), with K_D Cu(I) 5.47 x10^{-18} M (Fig. S3). (**g**) Microscale thermophoresis binding curves of copper transporter RAN1 with PLS. (**h**) Microscale thermophoresis binding curves of soluble copper chaperones ATX1 and CCH with PLS (n = 3, ±SD).

Fig. 1

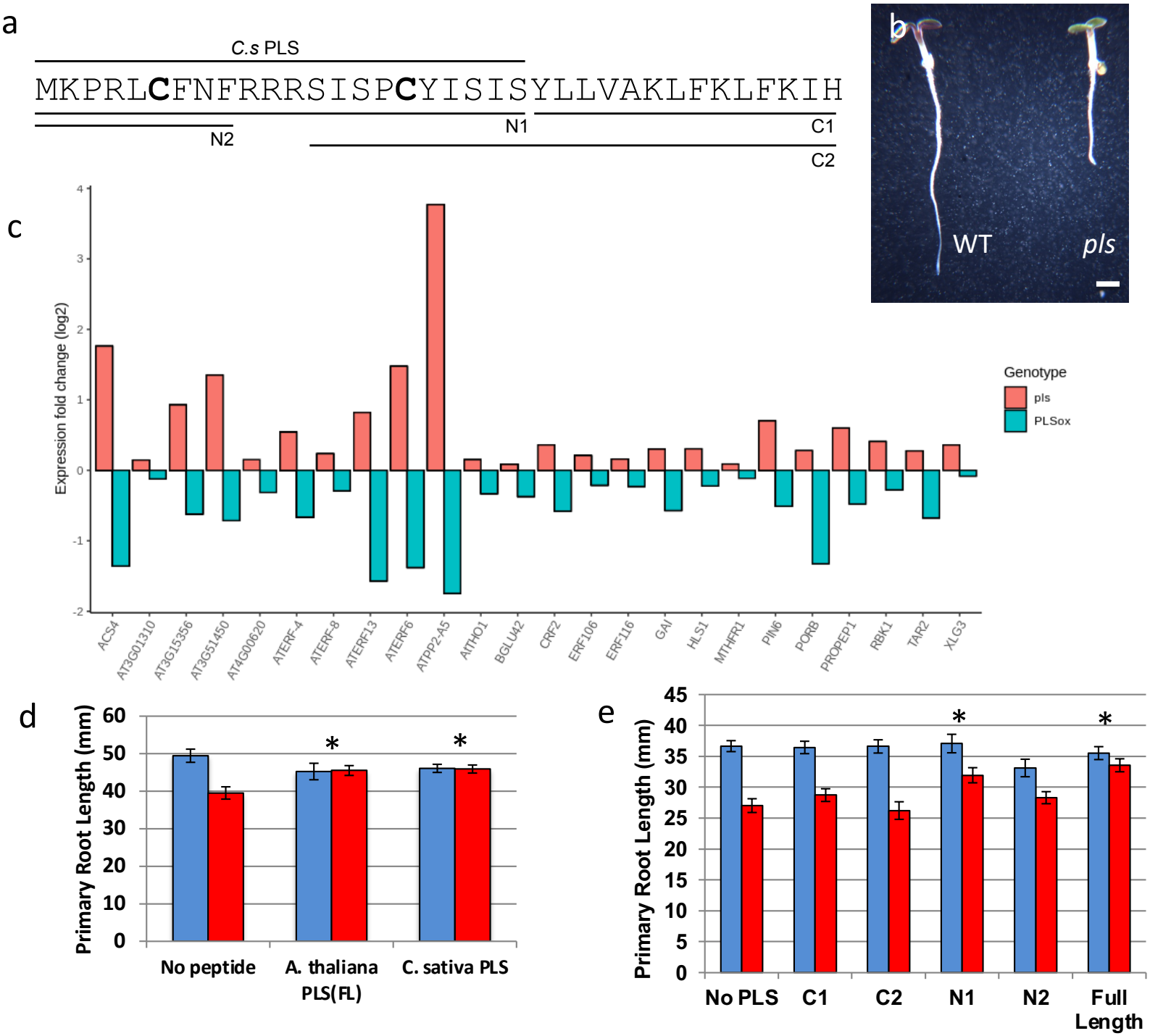
a
C.s PLS
MKPRLCFNFRRRSISPCYISISYLLVAKLFKLFKIH
N2
N1
C1
C2
b
WT
pls
c
Expression fold change (log2)
Genotype
pls
PLSox
ACS4
AT3G01310
AT3G15356
AT3G51450
AT4G00620
ATERF-4
ATERF-8
ATERF13
ATERF6
ATPP2-A5
AtTHO1
BGLU42
CRF2
ERF106
ERF116
GAI
HLS1
MTHFR1
PIN6
PORB
PROPEP1
RBK1
TAR2
XLG3
d
Primary Root Length (mm)
No peptide
A. thaliana PLS(FL)
C. sativa PLS
e
Primary Root Length (mm)
No PLS
C1
C2
N1
N2
Full Length

Figure 1. The PLS peptide is required for ethylene control of seedling growth, is structurally and functionally conserved, and complements the *Arabidopsis pls* mutant.

(**a**). Amino acid sequence of the PLS peptide from *Arabidopsis thaliana* with *Camelina sativa* PLS sequence (*C.s* PLS), and synthetic truncations N1, N2, C1 and C2, indicated by horizontal lines. Two cysteine residues are highlighted in bold. (**b**) Wildtype (left) and *pls* mutant (right); bar = 5 mm. (**c**) Expression levels of 24 ethylene-responsive genes in *pls* and *PLS* overexpressing seedlings, compared to wildtype levels. (**d**) Effect of *Arabidopsis* PLS full length peptide, *A.t.* PLS(FL), and *Camelina* PLS peptide (*C.s.* PLS) on *Arabidopsis* primary root length. Wildtype (C24) and *pls* mutant seedlings were grown hydroponically in the presence (100 nM) or absence of peptide for 10 d. Asterisks: ANOVA, $F_{2, 41} = 6.86$, $p = 0.003$; Tukey's HSD test. (**e**) Effect of PLS full length and truncated peptides on *Arabidopsis* primary root length. Seedlings were grown hydroponically in the presence of 50 nM peptide for 10 d. C1 = C-terminal 14 amino acids, C2 = C-terminal 24 amino acids, N1 = N-terminal 22 amino acids, N2 = N-terminal 9 amino acids, full length PLS = 36 amino acids. Asterisks: ANOVA, $F_{5,112} = 6.13$, $p = 4.65E\text{-}5$). Error bars show $\pm$ 1 standard error, n = 14-22.

Fig. 2

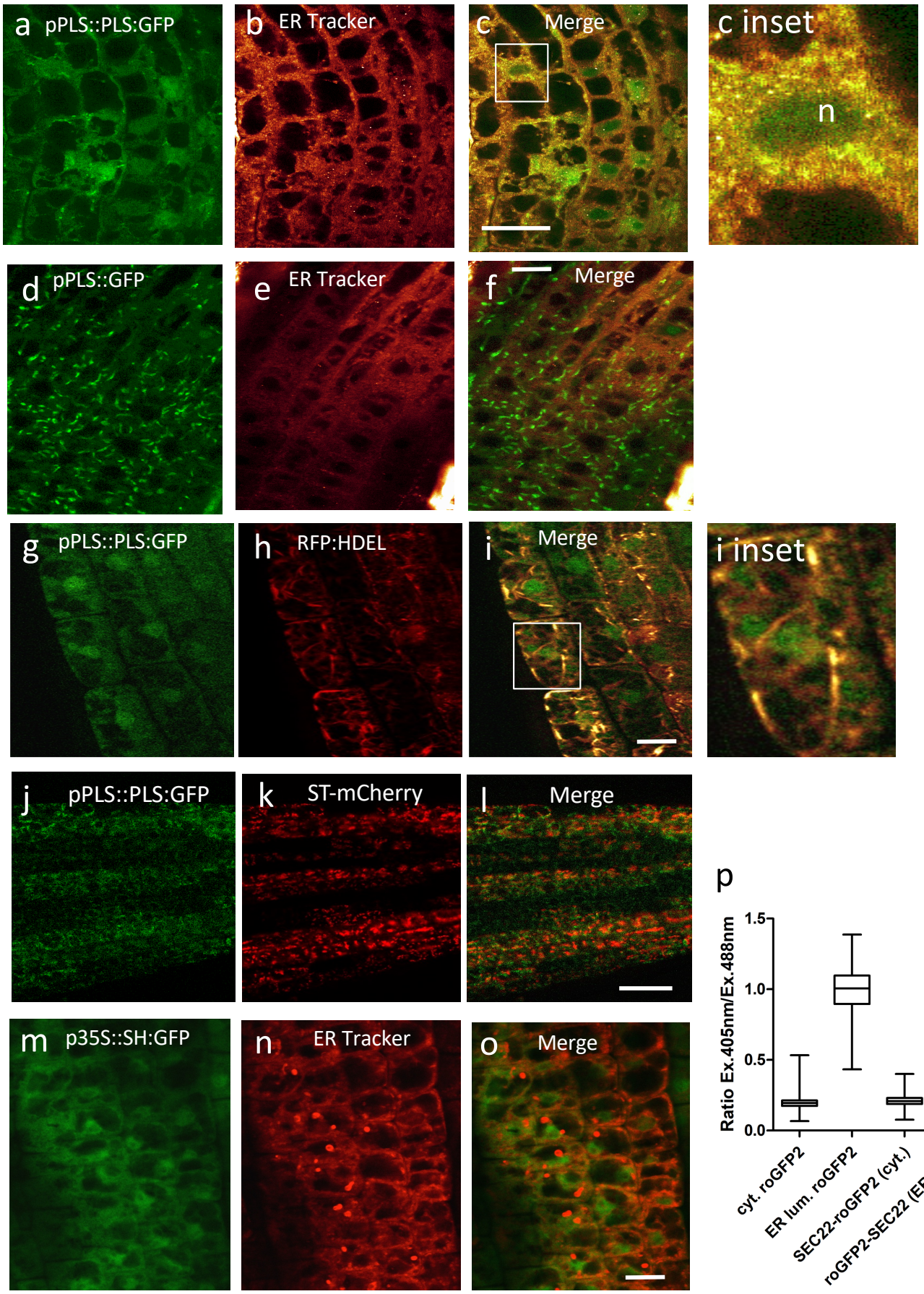

Figure 2. PLS localizes to the endoplasmic reticulum.
(**a-o**) PLS::PLS:GFP fusion protein (**a, g, j**) colocalizes with endoplasmic reticulum markers ER Tracker (**b, c, c inset**) and RFP:HDEL (**h, i, i inset**), but free GFP does not (**d-f**, **m-o**). PLS:GFP staining is seen also in nuclei (n). PLS::PLS:GFP (**j**) does not co-localize with the *trans*-Golgi markers ST-mCherry SH:GFP (**k, l**). Scale bars = 25 μm (**c, l**), 10 μm (**f, i, o**). (**p**) Ratiometric analysis of roGFP2 fusion constructs transiently expressed in *N. benthamiana*. Comparison of excitation ratios of PLS-roGFP2 and roGFP2-PLS with control constructs (free roGFP, SEC22 fusions) reveals that PLS localizes to the cytosolic side of the ER.

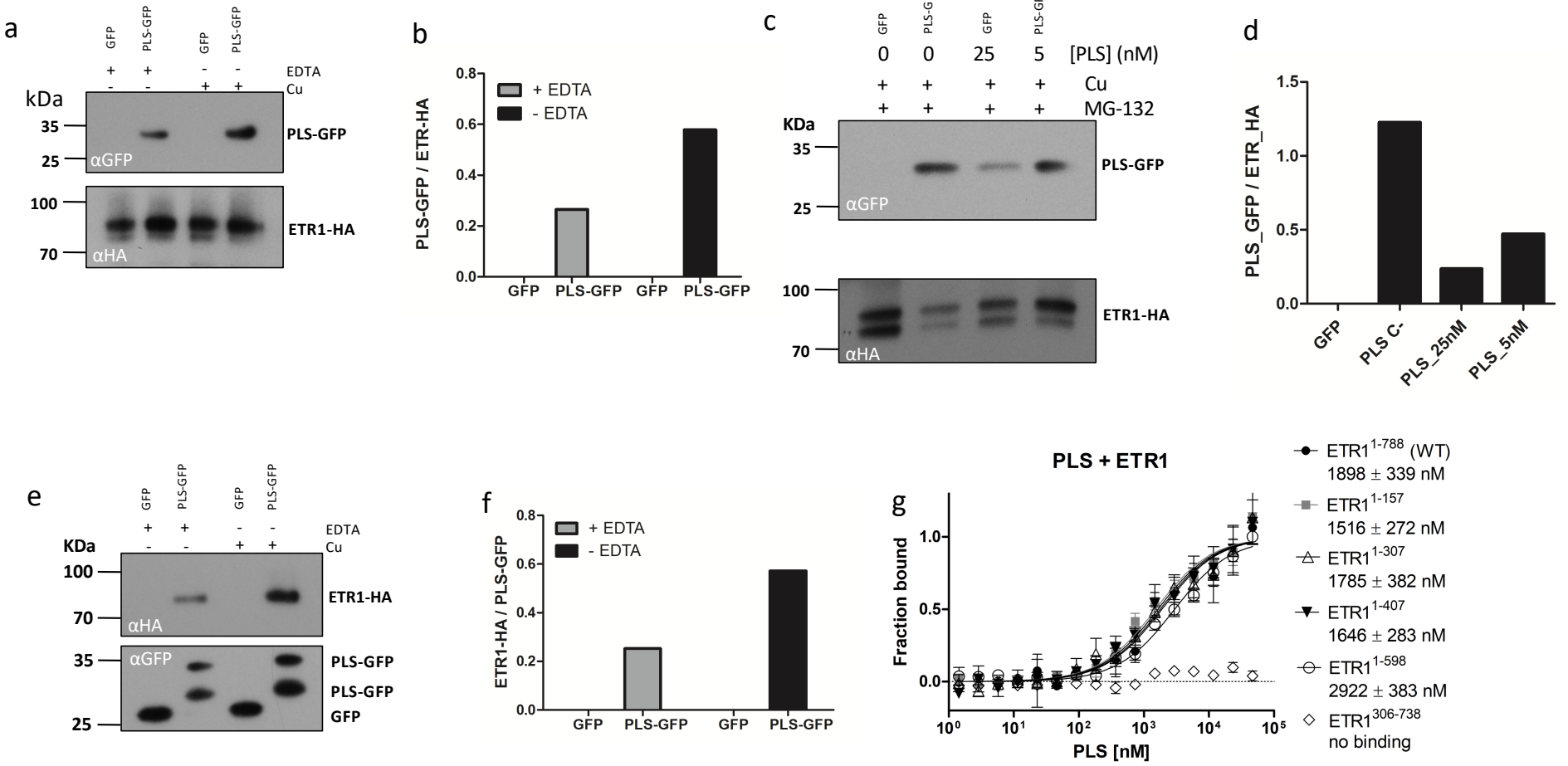
a
GFP
PLS-GFP
GFP
PLS-GFP
EDTA
Cu
kDa
35
25
αGFP
PLS-GFP
100
70
αHA
ETR1-HA
b
PLS-GFP / ETR-HA
+ EDTA
- EDTA
GFP
PLS-GFP
GFP
PLS-GFP
c
GFP
PLS-GFP
GFP
PLS-GFP
0
0
25
5
[PLS] (nM)
Cu
MG-132
KDa
35
25
αGFP
PLS-GFP
100
70
αHA
ETR1-HA
d
PLS_GFP / ETR_HA
GFP
PLS C-
PLS_25nM
PLS_5nM
e
GFP
PLS-GFP
GFP
PLS-GFP
EDTA
Cu
KDa
100
70
αHA
ETR1-HA
35
25
αGFP
PLS-GFP
PLS-GFP
GFP
f
ETR1-HA / PLS-GFP
+ EDTA
- EDTA
GFP
PLS-GFP
GFP
PLS-GFP
g
PLS + ETR1
Fraction bound
PLS [nM]
ETR1 1-788 (WT)
1898 ± 339 nM
ETR1 1-157
1516 ± 272 nM
ETR1 1-307
1785 ± 382 nM
ETR1 1-407
1646 ± 283 nM
ETR1 1-598
2922 ± 383 nM
ETR1 306-738
no binding

Fig. 3

Figure 3. PLS interacts with the ethylene receptor ETR1.
(**a**) Co-immunoprecipitation of PLS:GFP by ETR1:HA (upper panel) in leaves of *Nicotiana benthamiana*, in the presence and absence of 0.5 μM $CuSO_4$ and EDTA (to remove Cu). Lower panel shows presence of ETR1:HA in extracts using anti-HA antibody. (**b**) Densitometric scan of immunoblot. (**c**) Competition assay showing a reduced binding between PLS:GFP and ETR1:HA in the presence of 0, 5 nM or 25 nM PLS peptide, in the presence of 0.5 μM $CuSO_4$ and 50 μM MG-132, a proteasome inhibitor (upper panel). Lower panel shows ETR1:HA in extracts using anti-HA antibody. (**d**) Densitometric scan of immunoblot. (**e**) Co-immunopreciptation of ETR1:HA (upper panel) in leaves of *N. benthamiana*, showing the effect of EDTA (to remove Cu) on interaction between ERT1:HA and PLS:GFP. Lower panel shows presence of ETR1:HA in extracts using anti-HA antibody (**f**) Densitometric scan of immunoblot. α-GFP, anti-GFP antibody; α-HA, anti-HA antibody. (**g**) Microscale thermophoresis binding curves of different ETR1 truncations with PLS. Binding of PLS was observed with full-length ETR1 and all C-terminal truncations but not with $ETR1^{306-738}$ lacking the N-terminal transmembrane part of the receptor.

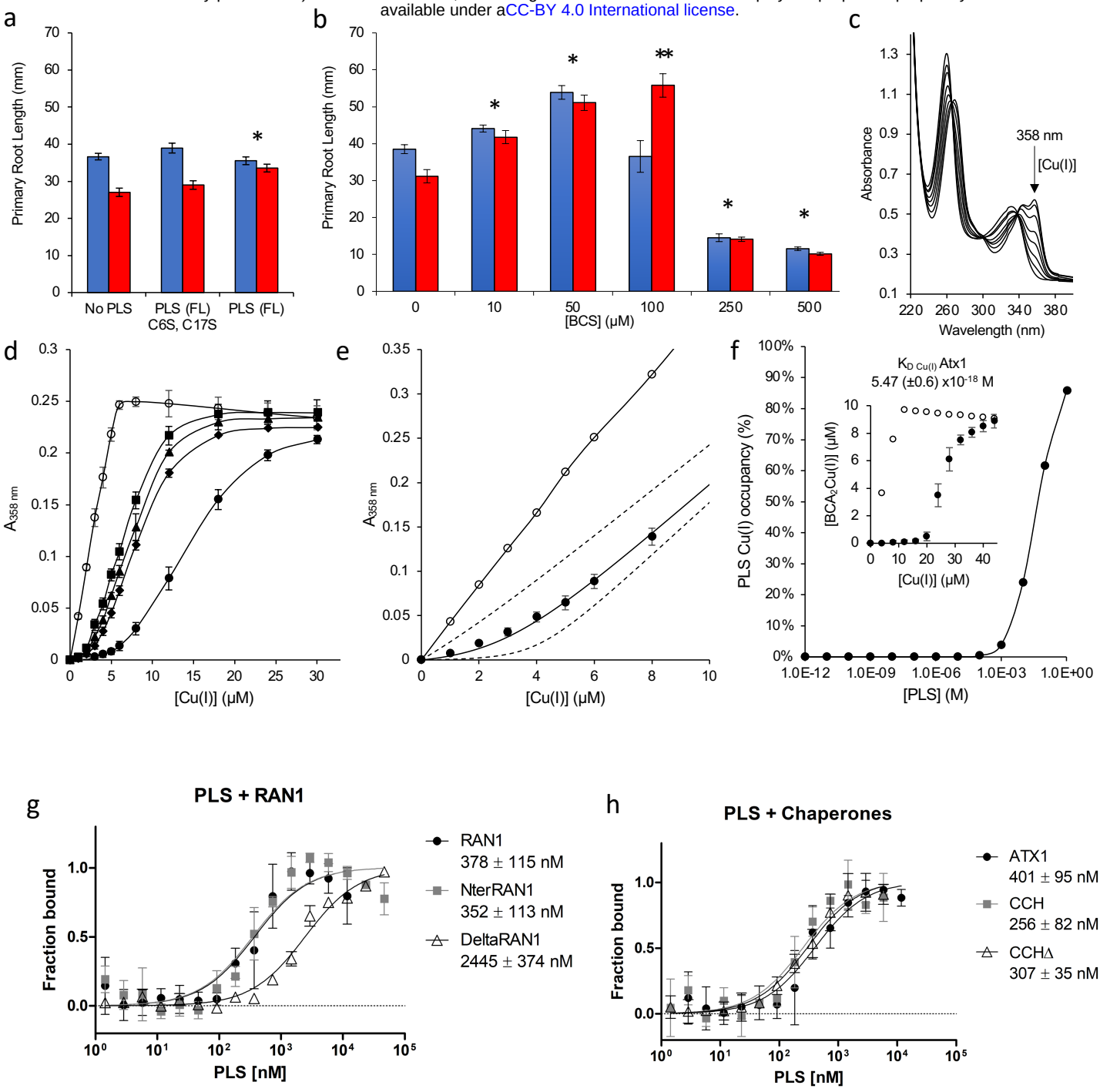

Fig. 4

Figure 4. PLS binds copper and interacts with RAN1 and copper chaperones.

(**a**) C6S and C17S in PLS are required for function. Seedlings were grown hydroponically for 10 d in the presence (100 nM) or absence of peptide (FL or C6S, C17S). Asterisk: ANOVA, $F_{2,\ 51} = 9.48$, p = 3.15E-4, Tukey's HSD). Error bars show ± 1 standard error, n = 14-22. Blue bars are C24, red bars are *pls*. (**b**) Effect of exogenous Cu(I) chelator BCS on primary root length of *Arabidopsis* grown hydroponically for 10 d. Asterisks: Student's t test analysis, $p < 0.005$. Error bars show ±1 standard error. (**c**) Absorption of BCA (17.3 µM) titrated with Cu(I) (representative spectrum, n = 2, full dataset Fig S1). (**d**) Binding isotherms ($A_{358\ nm}$) of BCA (10 µM) in the presence/absence (filled/empty symbols, respectively) of 14 µM MBP-PLS (circles) or MBP-PLS mutants (C6S, C17S and C6S/C17S: triangles, diamonds and squares respectively) titrated with Cu(I) (n = 3, ±SD). (**e**) Binding isotherms ($A_{358\ nm}$) of BCA (50 µM) in the presence/absence of 10 µM MBP-PLS (filled/empty symbols, respectively) titrated with Cu(I). Model (solid line) describes Cu(I)-binding as a 2:1 complex, with β_2 affinity of 3.79 (±1.5) $x10^{19}$ M^{-2}. Dotted lines simulate 10x weaker or tighter affinity (n = 3, ±SD). (**f**) Simulated Cu(I) occupancy (Supplementary Text) as a function of [PLS] using β_2 Cu(I) affinity of 3.79 $x10^{19}$ M^{-2}. Inset, *Arabidopsis* ATX1 (20 µM, filled circles) withholds one Cu(I) equivalent from 20 µM BCA (open circles, BCA-alone) (n = 3, ±SD), with K_D Cu(I) 5.47 $x10^{-18}$ M (Fig. S3). (**g**) Microscale thermophoresis binding curves of copper transporter RAN1 with PLS. (**h**) Microscale thermophoresis binding curves of soluble copper chaperones ATX1 and CCH with PLS (n = 3, ±SD).